

Applying narrowband remote-sensing reflectance models to wideband data

ZhongPing Lee

Northern Gulf Institute, Mississippi State University, Stennis Space Center,
Mississippi 39529, USA (zplee@ngi.msstate.edu)

Received 24 November 2008; revised 2 March 2009; accepted 11 March 2009;
posted 13 May 2009 (Doc. ID 104425); published 5 June 2009

Remote sensing of coastal and inland waters requires sensors to have a high spatial resolution to cover the spatial variation of biogeochemical properties in fine scales. High spatial-resolution sensors, however, are usually equipped with spectral bands that are wide in bandwidth (50 nm or wider). In this study, based on numerical simulations of hyperspectral remote-sensing reflectance of optically-deep waters, and using Landsat band specifics as an example, the impact of a wide spectral channel on remote sensing is analyzed. It is found that simple adoption of a narrowband model may result in >20% underestimation in calculated remote-sensing reflectance, and inversely may result in >20% overestimation in inverted absorption coefficients even under perfect conditions, although smaller (~5%) uncertainties are found for higher absorbing waters. These results provide a cautious note, but also a justification for turbid coastal waters, on applying narrowband models to wideband data. © 2009 Optical Society of America

OCIS codes: 010.0010, 010.1690, 010.4450, 280.4991.

1. Introduction

Ocean color remote sensing utilizes radiometric data to derive, empirically or analytically, desired information of subsurface constituents [1,2]. Operationally, two types of satellite sensors are commonly employed for the measurement of ocean color (spectral upwelling radiance from below the surface that emits to space). These sensors are contrasted by their specifics in data collection: one sensor (such as the Moderate Resolution Imaging Spectroradiometer (MODIS) [3]) has medium (or low) spatial resolution (a footprint of hundreds of meters or larger) with a narrow bandwidth (20 nm or narrower), while the other (such as the Landsat [4], IKONOS [5], Quick-Bird [6], or Advanced Land Observing Satellite (ALOS) [7]) has a high spatial resolution (a footprint of 30 m or finer) with a wide bandwidth (50 nm or wider). Because of such contrast in their sensor characteristics, the data collected by these sensors have different applicability. For remote sensing of oceanic waters, where in general, horizontal gradients of the

biogeochemical properties are mild, data with medium to low spatial resolution are sufficient [8]. For remote sensing of coastal and inland waters, however, due to reasons from small target areas to land/river runoff effects, it requires sensors with high spatial resolution to observe the intense geophysical variations within a short distance. Such a difference in the requirement of spatial resolution has an impact on sensor designs. Because the pixel size of medium-resolution data (MRD) is ~10–30 times larger than that of high-resolution data (HRD), a sensor for MRD is able to reduce the bandwidth of the spectral channels to about 10–20 nm and still maintain a high signal-to-noise ratio (SNR), which is critical for reliably deriving subsurface properties. For the case of HRD, there are two options to obtain higher SNR: one option is to increase the integration time, but this is impractical for polar orbiting satellites, and prolonged integration time will decrease the sharpness of an image; the other is to increase the bandwidth of the spectral channels, as demonstrated by the operational Landsat satellite, where the bandwidths are ~50–70 nm.

For coastal and inland remote sensing, HRD is required for meaningful and useful measurements

of water quality (such as concentration of chlorophyll, load of suspended sediments, and water clarity). Experimental sensors with both high spatial and spectral resolutions (such as Hyperion on EO1 [9]) have shown great promise for coastal remote sensing [10,11], but their SNRs are far from optimal for remote sensing of oceanic waters. Numerous studies have been carried out to obtain coastal biogeophysical information from Landsat measurements (e.g., Dekker *et al.* [12], Hellweger *et al.* [13], and Vincent *et al.* [14]). For the derivation of water-quality parameters from HRD, generally there are two schools of approaches: one is via empirical regressions (e.g., Vincent *et al.* [14], Zhang *et al.* [15], and Stumpf *et al.* [16]), and the other is via analytical or semi-analytical models (e.g., Dekker *et al.* [12], Doxaran *et al.* [17], and Heng *et al.* [18]). Empirical approaches basically compile concurrent (or near concurrent) *in situ* and satellite data and link the two data sources statistically to achieve optimal regression coefficients for a desired product (e.g., chlorophyll concentration or Secchi depth). The empirical coefficients from such exercises are normally best applicable to the research areas and/or to the seasons where the data are taken. They are, because of wide variations of bio-optical properties [19], in general, less applicable to other regions or at other seasons. To overcome such limitations and to better characterize product uncertainties, it is desired and useful to take approaches that are based on analytical or semi-analytical models.

For data from narrowband sensors (e.g., sea-viewing wide field-of-view sensor or MODIS), semi-analytical models [20,21] based on the radiative transfer equation have been developed to describe the remote-sensing reflectance (R_{rs} , sr⁻¹), which is defined as the ratio of water-leaving radiance (L_w , w/(m² nm sr)) to downwelling irradiance (E_d , w/(m² nm)) just above the surface, i.e.,

$$R_{rs}(\lambda_i^c) = \frac{L_w(\lambda_i^c)}{E_d(\lambda_i^c)}. \quad (1)$$

Here λ_i^c is the center wavelength of band i .

For optically-deep waters, the semi-analytical models for R_{rs} can be summarized into a generalized mathematical form [20]:

$$R_{rs}(\lambda_i^c) = G(\lambda_i^c) \frac{b_b(\lambda_i^c)}{a(\lambda_i^c) + b_b(\lambda_i^c)}. \quad (2)$$

Here G is a model parameter that varies with water's inherent optical properties (IOPs) [22], a (m⁻¹) is the total absorption coefficient, and b_b (m⁻¹) is the total backscattering coefficient. With models like this, various algorithms have been developed to retrieve sub-surface physical and biogeochemical properties [23–25].

There are no semi-analytical models developed specifically for R_{rs} from wide band sensors (WBS).

Usually the models developed for narrowband sensors are applied directly (e.g., Doxaran *et al.* [17]), with IOPs considered as their corresponding averages at each band, i.e.,

$$R_{rs}(\lambda_i^W) = \bar{G}(\lambda_i^W) \frac{\bar{b}_b(\lambda_i^W)}{\bar{a}(\lambda_i^W) + \bar{b}_b(\lambda_i^W)}. \quad (3)$$

Here \bar{b}_b and \bar{a} are band-averaged values at each WBS channel (λ_i^W). As model parameter G is commonly considered as a function of $b_b/(a + b_b)$ [20], $\bar{G}(\lambda_i^W)$ can be evaluated with the band-averaged \bar{b}_b and \bar{a} values.

For remote sensing by a WBS, however, the measured remote-sensing reflectance at band i is

$$R_{rs}(\lambda_i^W) = \frac{\int_{\lambda_i^l}^{\lambda_i^u} L_w(\lambda) d\lambda}{\int_{\lambda_i^l}^{\lambda_i^u} E_d(\lambda) d\lambda}. \quad (4)$$

with λ_i^l and λ_i^u the lower and upper wavelength boundaries for band i , respectively. Here the sensor's response function at each band is considered as a perfect boxcar function and then omitted in the expression and in this study. Based on Eqs. (1) and (2), the exact model formulation for remote-sensing reflectance of optically-deep water measured by a WBS is

$$R_{rs}(\lambda_i^W) = \int_{\lambda_i^l}^{\lambda_i^u} G(\lambda) \frac{b_b(\lambda)}{\kappa(\lambda)} E_d(\lambda) d\lambda / \int_{\lambda_i^l}^{\lambda_i^u} E_d(\lambda) d\lambda, \quad (5)$$

with $\kappa = a + b_b$.

Because $E_d(\lambda)$ is not spectrally constant, mathematically and strictly speaking,

$$R_{rs}(\lambda_i^W) \neq \int_{\lambda_i^l}^{\lambda_i^u} G(\lambda) \frac{b_b(\lambda)}{\kappa(\lambda)} d\lambda. \quad (6)$$

Furthermore, G , b_b , and κ (in particular the absorption spectrum) spectra are spectrally dependent (see Mobley [26]) and, from mathematical principles,

$$R_{rs}(\lambda_i^W) \neq \int_{\lambda_i^l}^{\lambda_i^u} G(\lambda) d\lambda \frac{\int_{\lambda_i^l}^{\lambda_i^u} b_b(\lambda) d\lambda}{\int_{\lambda_i^l}^{\lambda_i^u} \kappa(\lambda) d\lambda}. \quad (7)$$

Therefore,

$$R_{rs}(\lambda_i^W) \neq \bar{G}(\lambda_i^W) \frac{\bar{b}_b(\lambda_i^W)}{\bar{a}(\lambda_i^W) + \bar{b}_b(\lambda_i^W)}. \quad (8)$$

Consequently, if we want to utilize Eq. (3) (for the sake of simplicity) to represent R_{rs} data measured by a WBS, it is necessary and important to know how big the difference is between R_{rs} from Eq. (5) (the exact form) and R_{rs} from Eq. (3) (the approximation), how this difference varies with water properties, and the likely impacts when this simple form is

utilized for remote-sensing applications. To find out and to understand the potential uncertainties and impacts associated with the simple model, using Landsat band specifics as an example, $R_{rs}(\lambda_i^W)$ values between the simple form and the spectrally-resolved form are evaluated for various IOPs in this study, as are the impacts of Eq. (3) on IOP inversions when it is applied to WBS data.

2. Numerical Analysis

To evaluate the likely errors associated with the simple approximation [Eq. (3)], a series of numerical simulations with various hyperspectral IOP values were carried out. For this evaluation, a hyperspectral (400–900 nm, with an interval of 5 nm), nadir-viewing $R_{rs}(\lambda)$ is simulated first with the following equations [23]:

$$R_{rs} = \frac{0.52r_{rs}}{1 - 1.7r_{rs}}, \quad (9)$$

$$r_{rs} = \left(0.089 + 0.125 \frac{b_b}{\kappa}\right) \frac{b_b}{\kappa}. \quad (10)$$

Here r_{rs} is the nadir-viewing remote-sensing reflectance just below the sea surface, and wavelength dependence is omitted for brevity. b_{bw} and b_{bp} ($b_b = b_{bw} + b_{bp}$) are the backscattering coefficients of pure water and particles, respectively; κ includes the contributions of absorption coefficients of pure water (a_w), phytoplankton pigments (a_{ph}), and detritus plus colored dissolved organic matter (a_{dg}).

For the calculation of R_{rs} spectra, hyperspectral absorption and backscattering coefficients are generated with the following inputs: (1) Values of $a_w(\lambda)$ are from Pope and Fry [27] (400–695 nm) and Hale and Querry [28] (700–900 nm). a_w values of Hale and Querry are raised by 4% to match the a_w value of Pope and Fry at 700 nm. Figure 1 shows the a_w spectrum used in this study. (2) Values of $b_{bw}(\lambda)$ are from Morel [29]; (3) $a_{ph}(\lambda)$ is modeled as in Lee *et al.* [30]

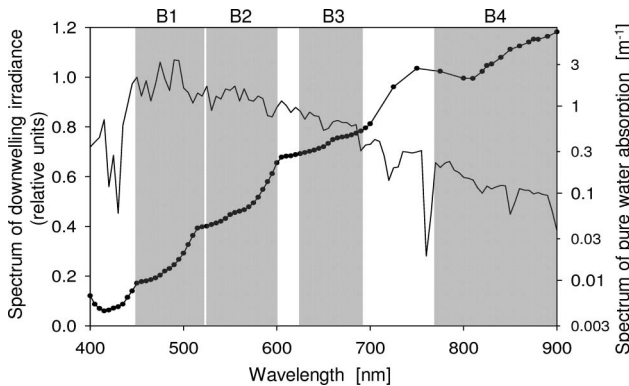


Fig. 1. Spectrum of pure water absorption coefficient (a_w) used in this study (line with dark circle). Also shown is a spectral shape of $E_d(\lambda)$ (thin line), modeled by MODTRAN with continental aerosols. The vertical bars indicate the four visible/near-infrared bands of Landsat.

with $a_{ph}(440)$ values ranging 0.005–5.0 m^{-1} . For $\lambda > 720$ nm, $a_{ph}(\lambda)$ is considered as equal to $a_{ph}(720)$. (4) $a_{dg}(\lambda)$ is modeled as an exponential function of wavelength [31] scaled by $a_{dg}(440)$, with a spectral slope of 0.019 nm^{-1} and $a_{dg}(440)$ values ranging 0.005–5.0 m^{-1} . (5) $b_{bp}(\lambda)$ is modeled as a power-law function of wavelength [19] scaled by $b_{bp}(440)$, with an exponent of 0.5 and $b_{bp}(440)$ values ranging 0.002–2.0 m^{-1} . A total of 12 sets of IOPs were created covering an $a(440)$ range of ~ 0.016 –10.0 m^{-1} and a $b_b(440)$ range of ~ 0.004 –2.0 m^{-1} , where $a(440)$ and $b_b(440)$ values are not covarying and cover the general range of oceanic and coastal waters [32]. As the focus here is to observe the potential uncertainties introduced by a simple model like Eq. (3), it is not necessary to carry out simulations with all possible combinations of IOPs observed in natural waters, although that might be required for the development of an optimal scheme to correct the wideband effects.

Landsat has four bands in the visible to near infrared that could be used for water remote sensing. The bands are Band 1 (450–520 nm), Band 2 (520–600 nm), Band 3 (630–690 nm), and Band 4 (770–900 nm). For these Landsat bands, the variation of $E_d(\lambda)$ within a band is less than $\sim 20\%$ (see Fig. 1). Further, because $R_{rs}(\lambda_i^W)$ is derived by normalizing the total L_w (which is proportional to E_d) to the total E_d within a band [see Eq. (4)], the impact on $R_{rs}(\lambda_i^W)$ from E_d spectral variation within a band is negligible ($< \sim 1\%$); therefore Eq. (5) can be well approximated as

$$R_{rs}(\lambda_i^W) \approx \int_{\lambda_i^l}^{\lambda_i^u} R_{rs}(\lambda) d\lambda. \quad (11)$$

With the simulated hyperspectral absorption and backscattering coefficients, it is now straightforward to calculate and compare $R_{rs}(\lambda_i^W)$ values from Eq. (3) and from Eqs. (9)–(11), respectively. To be consistent, $R_{rs}(\lambda_i^W)$ from Eq. (3) also utilized Eqs. (9) and (10), but simply with band-averaged total backscattering and total absorption coefficients as inputs. Note that here sensor's response function of each Landsat band is omitted as it is nearly flat spectrally (within $\pm 10\%$) for the primary portion of the bands [33].

If the sensor's response function significantly deviates from a perfect boxcar function, it should be included in the integrations of Eqs. (4) and (11) as in Bukata *et al.* [34]. Also, if a band covers the 400–450 nm range, or any other ranges that contain significant spectral variations of E_d , larger impacts on $R_{rs}(\lambda_i^W)$ from $E_d(\lambda)$ variation could be expected and a more strict formulation like Eq. (5) should be applied.

3. Results and Discussion

Figure 2 presents examples of simulated hyperspectral R_{rs} (solid line) and $R_{rs}(\lambda_i^W)$ calculated by Eq. (3) (open square) and by Eq. (11) (solid circle), respectively. These circles and squares represent R_{rs} at

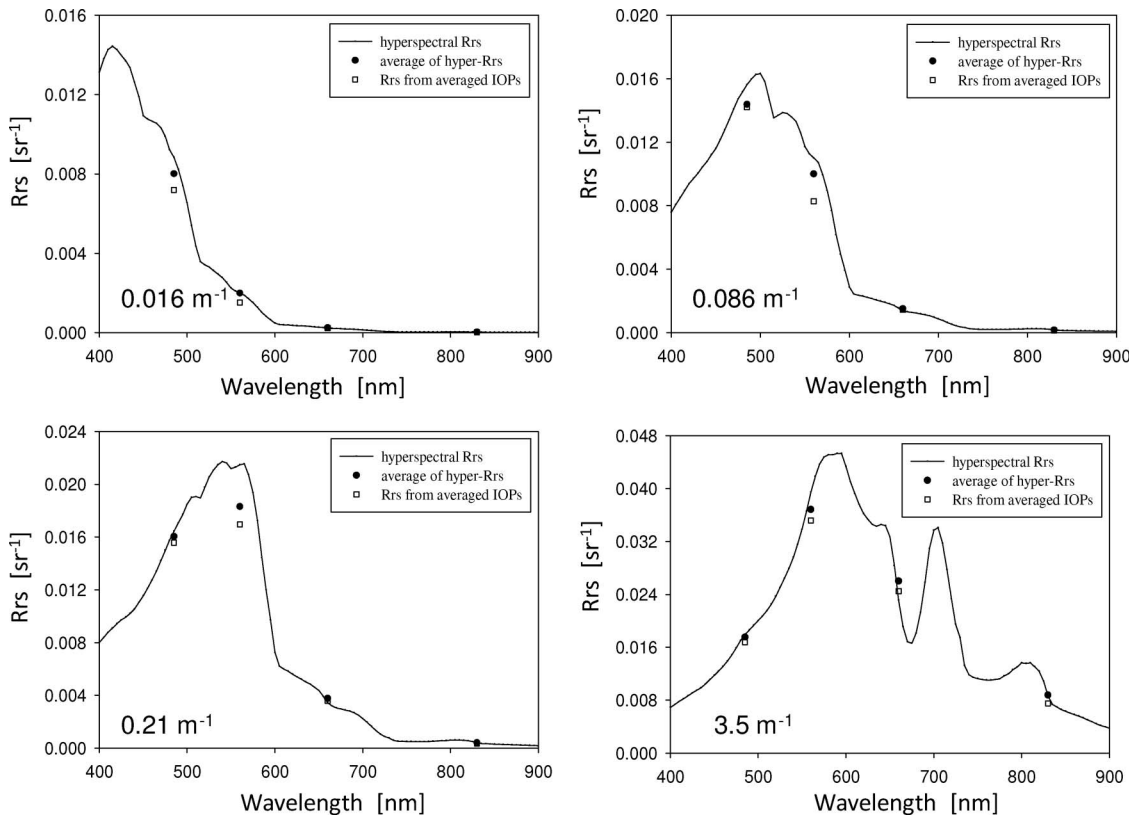


Fig. 2. Examples of simulated hyperspectral R_{rs} , along with $R_{rs}(\lambda_i^W)$ calculated by Eq. (3) (open square) and by Eq. (11) (solid circle). Values in each chart indicate the total absorption coefficients at 440 nm, which conceptually indicate that top left represents oceanic water, top right for offshore water, lower left for near-shore water, and lower right for coastal turbid water.

the center wavelengths of the Landsat bands. As demonstrated in Dekker *et al.* [12,35], expanding the bandwidth of the spectral channels will diminish the sharpness of the spectral features on which remote sensing of geophysical information relies. Furthermore, it is not surprising to see that values of $R_{rs}(\lambda_i^W)$ calculated from Eqs. (3) and (11) are different for various IOP combinations, and the differences are not uniform. To quantify the error of the simple approximation [Eq. (3)], Fig. 3 shows the percentage difference, $100 \times (\text{Eq. 3} - \text{Eq. 11}) / \text{Eq. 11}$, for $R_{rs}(\lambda_i^W)$ at the four Landsat bands, along with their relationships with the total absorption coefficient at 440 nm. It is found that all $R_{rs}(\lambda_i^W)$ from Eq. (3) are smaller than that from Eq. (11), and the difference can be as large as $\sim 24\%$. The differences at Bands 1–3 are much smaller ($\sim 5\%$), however, for relatively turbid waters ($a(440) > \sim 0.3 \text{ m}^{-1}$), which provide a fundamental justification of applying forms like Eq. (3) to WBS data over coastal turbid waters.

Because different IOPs (especially the spectral selective characteristics of the absorption coefficient) have different impacts on $R_{rs}(\lambda_i^W)$, errors associated with $R_{rs}(\lambda_i^W)$ at the four Landsat bands are not uniform. Both Band 1 (centered at 485 nm) and Band 2 (centered at 560 nm) experienced highest $R_{rs}(\lambda_i^W)$ difference between Eqs. (3) and (11) when there are fewer dissolved and/or suspended constituents in water. This is because there are sharp (about 4–5 times) in-

creases of absorption coefficients of pure water that Band 1 and Band 2 cover (see Fig. 1). These values dominate the total absorption coefficient when waters are clearer. Mathematically, for a series of values of x_i that contains wide range of lower to higher values, the inverse ($1/\bar{x}$) of the series' average (\bar{x}) is influenced more by the higher x_i values, while the

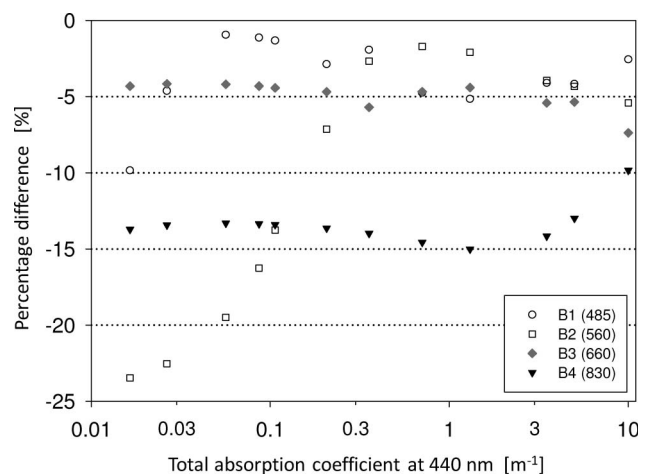


Fig. 3. Percentage difference between values of $R_{rs}(\lambda_i^W)$ calculated by Eq. (3) and by Eq. (11) for the four Landsat bands, respectively. Because of the limited numerical simulations, this chart is not intended to draw a definite relationship between the error and the total absorption coefficient, but to indicate the likely uncertainties for different IOPs.

average of the individual x_i 's inverse ($\overline{1/x_i}$) is influenced more by the lower x_i values. These facts explain why $R_{rs}(\lambda_i^W)$, which is in general inversely related to total absorption coefficient, by Eq. (3) is smaller than that by Eq. (11), and why there could be big difference between R_{rs} from Eq. (3) and R_{rs} from Eq. (11). Further, this fact implies that, if Eq. (3) is used for semianalytical retrieval of water's IOPs, the inverted total absorption coefficient of a wideband does not represent the band-averaged total absorption coefficient at that band (see below).

When there are more dissolved and suspended constituents (such as gelbstoff and phytoplankton) in water, because they contribute most to the absorption coefficients at the shorter wavelengths and the contributions are spectrally broad, the spectral feature of pure water absorption diminishes gradually. Consequently, the $R_{rs}(\lambda_i^W)$ error at Band 1 and Band 2 reduces to $\sim 5\%$.

At Band 3 (centered at 660 nm) and Band 4 (centered at 835 nm), on the other hand, because the contribution from pure water dominates the total absorption spectrum, the differences do not vary much across the various IOPs. The difference of $R_{rs}(\lambda_i^W)$ at Band 3, however, is smaller ($\sim 5\%$) than that at Band 4 ($\sim 15\%$), because at Band 3 a_w only varies in a range of $\sim 0.3\text{--}0.5\text{ m}^{-1}$, while at Band 4 it varies from ~ 2 to 6 m^{-1} .

To test the impact of wideband data and a simple wideband model [Eq. (3)] on IOP retrievals, Eq. (11)-simulated $R_{rs}(\lambda_i^W)$ were used as inputs to derive particle backscattering and total absorption coefficients following the quasi-analytical algorithm (QAA) approach [23,36]. In the process, Landsat Band 2 (with center wavelength of 560 nm) was considered as the reference wavelength [23], and the actual band-averaged total absorption coefficients were used, i.e., assuming a perfect estimation of absorption coefficient at the reference wavelength. With known $R_{rs}(B2)$ and $a(B2)$, $b_{bp}(B2)$ at this band can be derived algebraically as in Lee *et al.* [23]. Propagate this b_{bp} to Band 1 (with center wavelength of 485 nm) with the known exponent (0.5, again, assuming a perfect estimation), $a(B1)$ is then derived from known $R_{rs}(B1)$. Figure 4 compares the derived $a(B1)$ with the known band-averaged values (open circle) as well as $a(485)$ —the absorption coefficients at the center wavelength (dark square). Clearly, when no corrections are made for the wideband effects, it could result in 20% overestimation of $a(B1)$ even under ideal conditions. In reality, especially for complex coastal waters, larger uncertainties are associated with the estimation of the absorption coefficients at Band 2 and the exponent for the particle backscattering coefficient, and consequently larger uncertainties of remotely derived $a(B1)$ would be expected [37].

For waters with higher absorption coefficients ($a(B1) > \sim 0.2\text{ m}^{-1}$), however, the QAA inverted $a(B1)$ (under ideal conditions) are quite consistent (within $\pm 5\%$) with known $a(B1)$ values, at least for

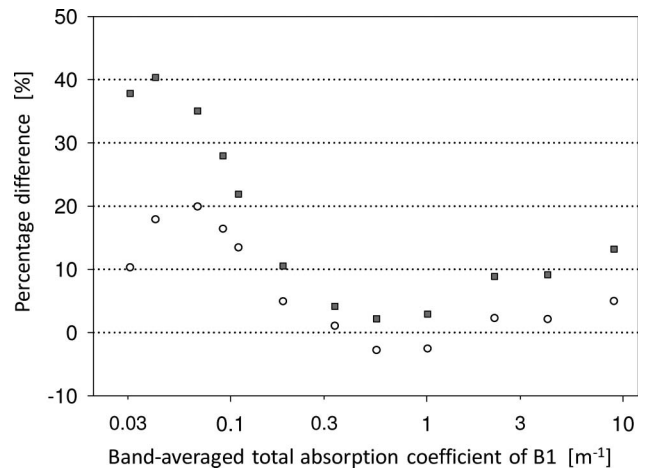


Fig. 4. Percentage difference, $[a_{\text{inversion}} - a_{\text{known}}]/a_{\text{known}} \times 100$, between inverted (using QAA with $B2$ as reference wavelength) $a(B1)$ and known absorption coefficients, for the same data used for Figs. 2 and 3. The X axis represents known band-averaged values of $a(B1)$. The dark-square symbol represents a comparison between inverted $a(B1)$ and the absorption at the center wavelength; the open-circle symbol represents a comparison between inverted $a(B1)$ and known $a(B1)$, i.e., a comparison of band-averaged values.

the limited data in this study. Such theoretical and numerical results provide a justification for applying narrowband semianalytical models with wideband data over turbid waters (e.g., Heng *et al.* [18]), although fine adjustments might be necessary to reflect band specifics and data characteristics. But, as indicated earlier, wideband derived absorption coefficients cannot be compared with narrowband measurements, where a systematic overestimation is expected (see Fig. 4, data with square symbol).

Note that the effects of wide bandwidth on atmospheric correction is not discussed here, as it is out of the scope of this study and that various approaches to achieve satisfactory atmosphere correction can be found in Hu *et al.* [38] and Liang *et al.* [39]. Because empirical approaches of remote sensing directly link desired products with sensor measured data, the bandwidth effects are implicitly imbedded in the empirical coefficients and, therefore, no extra correction is necessary. The derived empirical coefficients, however, are usually site, season, and sensor specific, and therefore not easily transferable and/or applicable globally.

4. Conclusions

Remote-sensing systems with high spatial resolution ($\sim 30\text{ m}$ or finer) capability are required for monitoring coastal and inland waters. Such systems usually carry sensors with spectral channels that are wide ($\sim 50\text{ nm}$ or wider) in bandwidth to achieve desired SNRs. For optically-deep waters, such a wide bandwidth can cause more than 20% underestimation in modeled values if a narrowband remote-sensing reflectance model with band-averaged IOPs are simply applied. Inversely, applying a narrowband model to wideband reflectance data may result in

20% overestimation of the inverted absorption coefficient, at least at Band 1 when water is relatively clear. The differences can be larger or smaller as they are dependent on IOPs, as well as on band location and bandwidth. For Landsat Bands 1–3, we found that for turbid waters ($a(440) > \sim 0.3 \text{ m}^{-1}$) the bandwidth-introduced uncertainties are relatively small (<5%), which justifies the applications [12,18] of narrowband semianalytical models with such wideband data for coastal remote sensing.

Since remote-sensing reflectance is, in general, inversely dependent on the absorption coefficient, underestimation of this reflectance is also expected if a narrowband remote-sensing model developed for optically shallow waters (e.g., Maritorena *et al.* [40], Lee *et al.* [41]) is simply applied to WBS data collected over shallow regions, and its analytical inversion will be more problematic because of the wideband effect and the limited spectral channels [42].

To achieve accurate vicarious calibrations [43], or to better retrieve water's physical and biogeophysical properties, however, the bandwidth related uncertainties need to be accounted for, especially when waters are relatively clearer. Separately, because the band specifications of many others (such as IKONOS, ALOS, and QuickBird) are nearly identical to that of Landsat, the results and conclusions presented here are, in general, applicable to those sensors.

I am very grateful for the support provided by NASA's Biology and Biogeochemistry Program and by the Naval Research Laboratory. The comments and suggestions from two anonymous reviewers and the editor are also greatly appreciated.

References

- IOCCG, "Remote sensing of ocean colour in coastal, and other optically-complex, waters," in *Reports of the International Ocean-Colour Coordinating Group, No.3*, S. Sathyendranath, ed. (IOCCG, 2000).
- IOCCG, "Why ocean colour? The societal benefits of ocean-colour technology," in *Reports of the International Ocean-Colour Coordinating Group, No. 7*, T. Platt, N. Hoepffner, V. Stuart, and C. Brown, eds. (IOCCG, 2008).
- URL: <http://modis.gsfc.nasa.gov/about/specifications.php>
- URL: <http://Landsat.usgs.gov/>
- URL: <http://www.geoeeye.com>
- URL: <http://www.digitalglobe.com>
- URL: <http://www.eorc.jaxa.jp/ALOS/en>
- IOCCG, "Status and plans for satellite ocean-color missions: considerations for complementary missions," in *Reports of the International Ocean-Colour Coordinating Group, No. 2*, J. A. Yoder, ed. (IOCCG, 1998).
- URL: <http://eros.usgs.gov/products/satellite/eo1.php>
- Z. P. Lee, B. Casey, R. Arnone, A. Weidemann, R. Parsons, M. J. Montes, B.-C. Gao, W. Goode, C. O. Davis, and J. Dye, "Water and bottom properties of a coastal environment derived from Hyperion data measured from the EO-1 spacecraft platform," *J. Appl. Remote Sens.* **1**, 011502 (2007).
- V. E. Brando and A. G. Dekker, "Satellite hyperspectral remote sensing for estimating estuarine and coastal water quality," *IEEE Trans. Geosci. Remote Sens.* **41**, 1378–1387 (2003).
- A. G. Dekker, R. J. Vos, and S. W. M. Peters, "Analytical algorithms for lake water TSM estimation for retrospective analyses of TM and SPOT sensor data," *Int. J. Remote Sensing* **23**, 15–35 (2002).
- F. L. Hellweger, P. Schlosser, U. Lall, and J. K. Weissel, "Use of satellite imagery for water quality studies in New York Harbor," *Remote Sens. Environ.* **61**, 437–448 (2004).
- R. K. Vincent, X. Qin, R. M. L. McKay, J. Miner, K. Czajkowski, J. Savino, and T. Bridgeman, "Phycocyanin detection from LANDSAT TM data for mapping cyanobacterial blooms in Lake Erie," *Remote Sens. Environ.* **89**, 381–392 (2004).
- Y. Zhang, J. T. Pulliainen, S. S. Koponen, and M. T. Hallikaine, "Water quality retrievals from combined Landsat TM data and ERS-2 SAR data in the Gulf of Finland," *IEEE Trans. Geosci. Remote Sens.* **41**, 622–629 (2003).
- R. P. Stumpf, K. Holderied, and M. Sinclair, "Determination of water depth with high-resolution satellite imagery over variable bottom types," *Limnol. Oceanogr.* **48**, 547–556 (2003).
- D. Doxaran, J.-M. Froidefond, S. Lavender, and P. Castaing, "Spectral signature of highly turbid waters: application with SPOT data to quantify suspended particulate matter concentrations," *Remote Sens. Environ.* **81**, 149–161 (2002).
- A. W.-C. Heng, S. C. Liew, and C. W. Chang, "Retrieval of inherent optical properties from Landsat ETM+ data: possibilities and limitations," in *Proceedings of 2004 IEEE International Geoscience and Remote Sensing Symposium (IEEE, 2004)*, pp. 3487–3488.
- H. R. Gordon and A. Morel, *Remote Assessment of Ocean Color for Interpretation of Satellite Visible Imagery: A Review* (Springer-Verlag, 1983).
- H. R. Gordon, O. B. Brown, R. H. Evans, J. W. Brown, R. C. Smith, K. S. Baker, and D. K. Clark, "A semianalytic radiance model of ocean color," *J. Geophys. Res.* **93**, 10,909–10,924 (1988).
- Z. P. Lee, K. L. Carder, and K. P. Du, "Effects of molecular and particle scatterings on model parameters for remote-sensing reflectance," *Appl. Opt.* **43**, 4957–4964 (2004).
- R. W. Preisendorfer, *Hydrologic Optics Vol. 1: Introduction* (National Technical Information Service, 1976).
- Z. P. Lee, K. L. Carder, and R. Arnone, "Deriving inherent optical properties from water color: a multi-band quasi-analytical algorithm for optically deep waters," *Appl. Opt.* **41**, 5755–5772 (2002).
- S. Maritorena, D. A. Siegel, and A. R. Peterson, "Optimization of a semianalytical ocean color model for global-scale applications," *Appl. Opt.* **41**, 2705–2714 (2002).
- K. L. Carder, F. R. Chen, Z. P. Lee, S. K. Hawes, and D. Kamykowski, "Semianalytic moderate-resolution imaging spectrometer algorithms for chlorophyll-a and absorption with bio-optical domains based on nitrate-depletion temperatures," *J. Geophys. Res.* **104**, 5403–5421 (1999).
- C. D. Mobley, *Light and Water: Radiative Transfer in Natural Waters* (Academic, 1994).
- R. Pope and E. Fry, "Absorption spectrum (380–700 nm) of pure waters: II. Integrating cavity measurements," *Appl. Opt.* **36**, 8710–8723 (1997).
- G. M. Hale and M. R. Querry, "Optical constants of water in the 200 nm to 200 μm wavelength region," *Appl. Opt.* **12**, 555–563 (1973).
- A. Morel, "Optical properties of pure water and pure sea water," in *Optical Aspects of Oceanography*, N. G. Jerlov and E. S. Nielsen, ed. (Academic, 1974), pp. 1–24.
- Z. P. Lee, K. L. Carder, C. D. Mobley, R. G. Steward, and J. S. Patch, "Hyperspectral remote sensing for shallow waters. 1. A semianalytical model," *Appl. Opt.* **37**, 6329–6338 (1998).
- A. Bricaud, A. Morel, and L. Prieur, "Absorption by dissolved organic matter of the sea (yellow substance) in the UV and visible domains," *Limnol. Oceanogr.* **26**, 43–53 (1981).

32. J. T. O. Kirk, *Light and Photosynthesis in Aquatic Ecosystems* (Cambridge University, 1994).
33. URL: <http://Landsathandbook.gsfc.nasa.gov/>
34. R. P. Bukata, J. H. Jerome, K. Y. Kondratyev, and D. V. Pozdnyakov, *Optical Properties and Remote Sensing of Inland and Coastal Waters* (CRC Press, 1995).
35. A. G. Dekker, T. J. Malthus, M. M. Wijnen, and E. Seyhan, "The effect of spectral bandwidth and positioning on the spectral signature analysis of inland waters," *Remote Sens. Environ.* **41**, 211–225 (1992).
36. Z. P. Lee, A. Weidemann, J. Kindle, R. Arnone, K. L. Carder, and C. Davis, "Euphotic zone depth: Its derivation and implication to ocean-color remote sensing," *J. Geophys. Res.* **112**, C03009 (2007).
37. IOCCG, "Remote sensing of inherent optical properties: fundamentals, tests of algorithms, and applications," in *Reports of the International Ocean-Colour Coordinating Group, No. 5*, Z.-P. Lee, ed. (IOCCG, 2006), p. 126.
38. C. Hu, F. E. Muller-Karger, S. Andrefouet, and K. L. Carder, "Atmospheric correction and cross-calibration of LANDSAT-7/ETM + imagery over aquatic environments: a multiplatform approach using SeaWiFS/MODIS," *Remote Sens. Environ.* **78**, 99–107 (2001).
39. S. Liang, H. Fang, and M. Chen, "Atmospheric correction of Landsat ETM + Land surface imagery—part I: methods," *IEEE Trans. Geosci. Remote Sens.* **39**, 2490–2498 (2001).
40. S. Maritorena, A. Morel, and B. Gentili, "Diffuse reflectance of oceanic shallow waters: influence of water depth and bottom albedo," *Limnol. Oceanogr.* **39**, 1689–1703 (1994).
41. Z. P. Lee, K. L. Carder, C. D. Mobley, R. G. Steward, and J. S. Patch, "Hyperspectral remote sensing for shallow waters: 2. Deriving bottom depths and water properties by optimization," *Appl. Opt.* **38**, 3831–3843 (1999).
42. Z. P. Lee and K. L. Carder, "Effect of spectral band numbers on the retrieval of water column and bottom properties from ocean color data," *Appl. Opt.* **41**, 2191–2201 (2002).
43. R. E. Eplee, W. D. Robinson, S. W. Bailey, D. K. Clark, P. J. Werdell, M. Wang, R. A. Barnes, and C. R. McClain, "Calibration of SeaWiFS. II. Vicarious techniques," *Appl. Opt.* **40**, 6701–6718 (2001).